Journal of Zhejiang University-SCIENCE B in press
www.jzus.zju.edu.cn; www.springer.com/journal/11585
E-mail: jzus_b@zju.edu.cn

Research Article
https://doi.org/10.1631/jzus.B2600724

SCAP K210 lactylation is associated with SREBP1 signaling and lipid remodeling in TNBC

Guimei JI[1,2], Ting WEN[1,2], Yudi ZHANG[1,2], Xiaoqian JIA[1,2], Shuo RU[1,2], Yingying LI[1,2], Yuran DUAN[2,3], Zheng WANG[1,2], Daqian XU[1,2,4]✉, Zhiqiang HU[1,2]✉

[1]*Zhejiang Provincial Key Laboratory of Pancreatic Disease, The First Affiliated Hospital, Institute of Translational Medicine, Zhejiang University School of Medicine, Zhejiang University, Hangzhou 310029, China*
[2]*Zhejiang Key Laboratory of Frontier Medical Research on Cancer Metabolism, Zhejiang University, Hangzhou 310029, China*
[3]*Key Laboratory of Precision Diagnosis and Treatment for Hepatobiliary and Pancreatic Tumor of Zhejiang Province, Department of Hepatobiliary and Pancreatic Surgery, The Second Affiliated Hospital, School of Medicine, Zhejiang University, Hangzhou 310009, China*
[4]*NHC Key Laboratory of Cell Transplantation, Harbin Medical University, Harbin 150001, China*

Abstract: Metabolic reprogramming, as a hallmark of triple-negative breast cancer (TNBC), contributes to therapeutic adaptation. Lactate accumulation, a prominent feature of tumor metabolism, can regulate cellular functions through protein lactylation; however, the molecular targets and functional consequences of lactylation in TNBC remain incompletely understood. Here, we identified the sterol regulatory element-binding protein (SREBP) cleavage-activating protein (SCAP) as a lactate-responsive lactylation substrate in TNBC cells. Mass spectrometry analysis revealed lysine 210 (K210) as an evolutionarily conserved lactylation site on SCAP. Sodium lactate treatment was associated with an increased nuclear SREBP1 signal, increased sterol regulatory element (SRE)-dependent transcriptional activity, enhanced expression of the lipogenic enzymes fatty acid synthase (FASN) and stearoyl-CoA desaturase 1 (SCD1), and elevated neutral lipid accumulation. Reconstitution with the SCAP K210R mutant (lysine-to-arginine substitution at residue 210) markedly attenuated SREBP1-associated responses and neutral-lipid accumulation. Lactate reduced SCAP association with insulin-induced gene 1 (INSIG1), and this change was attenuated by K210R. Intracellular trafficking and SREBP1 proteolytic processing were not directly measured. In TNBC xenograft models, doxorubicin treatment increased SCAP-associated lactylation more prominently in wild-type than K210R tumors. K210R reconstitution reduced the basal tumor burden and, in combination with doxorubicin, produced the most pronounced tumor suppression, with a significant genotype × doxorubicin × time interaction for log-transformed tumor volumes, but no significant genotype × doxorubicin interaction for endpoint tumor weights. Collectively, our findings link SCAP K210 lactylation with lactate-responsive SREBP1-associated lipid remodeling in TNBC. The proposed trafficking mechanism and its specific role in doxorubicin resistance require further validation.

Key words: Triple-negative breast cancer; Lipid metabolism; Sterol regulatory element-binding protein (SREBP); SREBP cleavage-activating protein (SCAP); Lactylation; Doxorubicin response

✉ Zhiqiang HU, zhiqianghu@zju.edu.cn
Daqian XU, xudaqian@zju.edu.cn
Zhiqiang HU, https://orcid.org/ 0000-0003-1313-3470
Daqian XU, https://orcid.org/ 0000-0003-0478-2997
Guimei JI, https://orcid.org/0009-0008-0235-2495

Received Sept. 19, 2026; Revision accepted Nov. 7, 2026;
Crosschecked xxx. xx, 20xx

© Zhejiang University Press 2026

Unedited

1 Introduction

Triple-negative breast cancer (TNBC), defined by the absence of estrogen receptor, progesterone receptor, and human epidermal growth factor receptor 2, represents a clinically aggressive and molecularly heterogeneous subtype of breast cancer (Cancer Genome Atlas Network, 2012; Lehmann et al., 2016; Garrido-Castro et al., 2019; Asleh et al., 2022). Although the development of molecular classification and therapeutic strategies has greatly improved our understanding of TNBC biology, effective targeted treatments remain limited, and cytotoxic chemotherapy continues to represent the primary therapeutic modality (Mehanna et al., 2019; Marra et al., 2020). Compared with other breast cancer subtypes, TNBC displays pronounced biological plasticity, enabling tumor cells to adapt to fluctuating microenvironmental conditions and therapeutic stress. Increasing evidence suggests that metabolic reprogramming is a fundamental feature supporting TNBC progression and treatment adaptation (Wang et al., 2020; Munkácsy et al., 2023). Specifically, the aberrant accumulation and remodeling of lipids have emerged as important characteristics of TNBC (Li et al., 2023; Yu et al., 2024; Cai et al., 2025), suggesting that altered lipid metabolism may provide a critical metabolic advantage for tumor growth and survival.

Lipids serve not only as essential structural components but also as signaling molecules that regulate multiple aspects of cancer biology, including membrane organization, energy storage, redox homeostasis, as well as signal transduction (Jin et al., 2023; Taborda Ribas et al., 2024). Enhanced lipid synthesis and accumulation in TNBC have been associated with increased proliferative capacity, metastatic potential, and resistance to therapeutic stress (Sirois et al., 2019; Tan et al., 2023; Yu et al., 2024; Cai et al., 2025). Frequently activated oncogenic pathways in TNBC, including phosphoinositide 3-kinase (PI3K)–AKT–mechanistic target of rapamycin (mTOR) signaling, promote anabolic lipid metabolism by stimulating transcriptional programs that support fatty acid and cholesterol biosynthesis (Yamauchi et al., 2011; Yi et al., 2020). Consistently, pharmacological or genetic inhibition of lipid metabolic pathways have been shown to impair TNBC growth and enhance therapeutic sensitivity (Menendez and Lupu, 2017; Tracz-Gaszewska and Dobrzyn, 2019; Liang et al., 2023; Nuzzo et al., 2025). However, the regulatory mechanisms that drive lipid metabolic adaptation in TNBC remain unclear.

The sterol regulatory element-binding protein (SREBP) family represents a central transcriptional system controlling lipid biosynthesis. SREBP1 preferentially regulates genes involved in fatty acid synthesis, whereas SREBP2 primarily governs cholesterol biosynthesis (Yang et al., 2002; Brown et al., 2018; Cai et al., 2019; Zhao et al., 2022). The activation of SREBPs requires sterol regulatory element-binding protein cleavage-activating protein (SCAP), an escort protein that senses metabolic cues and mediates SREBP trafficking from the endoplasmic reticulum (ER) to the Golgi apparatus for proteolytic activation (Sun et al., 2005; Brown et al., 2018). Under sterol-replete conditions, the interaction between SCAP and insulin-induced gene 1 (INSIG1) retains the SCAP–SREBP complex in the ER, thereby preventing SREBP activation (Yang et al., 2002; Dong et al., 2012; Sun et al., 2005). Emerging studies have demonstrated that post-translational modifications of SREBP or SCAP can modulate this regulatory checkpoint. For example, the glucose-dependent N-glycosylation of SCAP reduces SCAP–INSIG1 association and promotes SREBP1 activation (Cheng et al., 2015, 2016), whereas other metabolic cues, such as ammonia-induced SCAP–INSIG dissociation and phosphoenolpyruvate carboxykinase 1 (PCK1)-mediated phosphorylation of INSIG proteins, can regulate SCAP trafficking and lipogenic signaling (Xu et al., 2020; Cheng et al., 2022). These findings suggest that metabolite-responsive protein modifications may represent an important mechanism linking cellular metabolic states to lipid metabolic reprogramming. Cancer-focused analyses have also considered the SCAP/SREBP pathway as a potential metabolic target, providing broader context for its relevance in tumor biology (Cheng et al., 2018).

Unedited

Lactate is increasingly recognized as a key metabolic regulator that contributes to TNBC progression. Traditionally considered a byproduct of aerobic glycolysis, lactate is currently appreciated as a versatile metabolite that functions as an energy substrate, signaling molecule, and regulator of the tumor microenvironment (Faubert et al., 2017; Chen et al., 2024b; Chen et al., 2025). Elevated lactate levels within tumors can promote malignant behaviors, including proliferation, invasion, immune evasion, and therapeutic resistance (Chen et al., 2024b; Gu et al., 2025; Luqmani, 2026). Beyond its metabolic and signaling functions, lactate can also serve as a substrate for lysine lactylation, a post-translational modification initially identified on histones that links glycolytic activity to transcriptional regulation (Zhang et al., 2019; Izzo and Wellen, 2019). Subsequent studies have revealed the extensive lactylation of non-histone proteins, suggesting that lactate can directly modify functional proteins to reshape cellular states (Yang et al., 2023; Chen et al., 2024a; Li et al., 2024; Peng and Du, 2025; Zhang et al., 2025b). Importantly, lactate has also been implicated in promoting lipid biosynthesis (Ippolito et al., 2022; Singh et al., 2023; Jin et al., 2023), although the molecular mechanisms connecting lactate accumulation to lipid metabolic regulation remain poorly defined. Whether lactate-induced lactylation directly modifies the key regulators of lipid synthesis and drives TNBC progression is yet to be determined.

Anthracycline chemotherapy, including doxorubicin, remains a cornerstone treatment for TNBC; however, therapeutic resistance frequently limits long-term efficacy (Nedeljković and Damjanović, 2019; Marra et al., 2020). Recent studies suggest that chemotherapy-induced metabolic stress can reshape the tumor microenvironment, including alterations in lactate production and accumulation (Sun et al., 2025; Li et al., 2026). Given that lactate can function as a substrate for protein lactylation, chemotherapy-induced lactate elevation may provide a mechanism by which tumor cells acquire adaptive metabolic programs through the modification of key regulatory proteins (Sun et al., 2025; Li et al., 2026; Zhang et al., 2025a). Therefore, identifying lactylated proteins that mediate lipid metabolic adaptation may reveal previously unrecognized mechanisms underlying TNBC chemoresistance.

Here, we investigated SCAP lactylation as a potential link between lactate availability and SREBP1-associated lipid phenotypes in TNBC. Liquid chromatography–tandem mass spectrometry (LC-MS/MS) was used to identify a lactylated SCAP peptide containing K210 in one independently prepared sample, and comparison with the SCAP K210R mutant (lysine-to-arginine substitution at residue 210) associated this residue with lactate-responsive SCAP lactylation and downstream cellular responses. Lactate treatment was linked to reduced SCAP–INSIG1 co-recovery and increased SREBP1-associated readouts, while direct SCAP trafficking and SREBP1 cleavage were not measured. In xenografts, K210R was associated with reduced tumor burden. Longitudinal tumor-volume analyses indicated different relative growth profiles among genotypes and treatment groups, but endpoint tumor-weight analysis did not show a significant genotype × doxorubicin interaction. These findings support the need to further investigate SCAP K210 in lactate-responsive lipid regulation without establishing a direct trafficking mechanism or doxorubicin resistance.

2 Materials and methods

2.1 Antibodies and reagents

The antibodies relevant to this study included anti-SCAP (ab125186, Abcam, Cambridge, UK), anti-INSIG1 (22115-1-AP, Proteintech), anti-tubulin (sc-8035, Santa Cruz Biotechnology, Dallas, TX, USA), mouse anti-Flag (F1804, Sigma-Aldrich, St Louis, MO, USA), rabbit anti-Flag (F7425, Sigma-Aldrich), and anti-Flag M2 agarose beads (Sigma-Aldrich). Normal mouse IgG (sc-2025) and normal rabbit IgG (sc-2027) were obtained from Santa Cruz Biotechnology. The antibodies against SREBP1 included anti-SREBP1 (ab28481, Abcam) and anti-SREBF1 (14088-1-AP, Proteintech). The pan-

Uncorrected

lysine-lactylation antibody (anti-L-lactyllysine rabbit monoclonal antibody, Cat. No. PTM-1401RM) was purchased from PTM Bio (Hangzhou, China). Hoechst 33342 (trihydrochloride, trihydrate, 10 mg/mL solution in water, Cat. No. H3570) was purchased from Invitrogen (Thermo Fisher Scientific). Sodium lactate (Cat. No. L7022) and doxorubicin hydrochloride (Cat. No. PHR1789) were obtained from Sigma-Aldrich (Merck, Darmstadt, Germany). BODIPY™ 493/503 (4,4-Difluoro-1,3,5,7,8-Pentamethyl-4-Bora-3a,4a-Diaza-s-Indacene, Cat. No. D3922) was purchased from Invitrogen (Thermo Fisher Scientific). The following fluorescent secondary antibodies were obtained from Thermo Fisher Scientific: Alexa Fluor™ 488-conjugated goat anti-rabbit IgG (Cat. No. A-11034), Alexa Fluor™ 546-conjugated goat anti-rabbit IgG (Cat. No. A-11035), Alexa Fluor™ 488-conjugated goat anti-mouse IgG (Cat. No. A-11029), and Alexa Fluor™ 546-conjugated goat anti-mouse IgG (Cat. No. A-11003). Unless otherwise specified, primary antibodies were used at 1:1000 for immunoblotting and 1:500 for immunoprecipitation. Horseradish peroxidase (HRP)-conjugated secondary antibodies were used at 1:5000.

2.2 Cell culture and transfection

Human MDA-MB-231 cells were obtained from the American Type Culture Collection (ATCC) and cultured in Dulbecco's modified Eagle's medium supplemented with 10% dialyzed bovine calf serum (HyClone) at 37°C in a humidified incubator containing 5% CO_2. Cells were seeded at 4×10^5 cells per 60-mm dish or 1×10^5 cells per well of a six-well plate approximately 18 h before transfection. Plasmid transfection was performed using Lipo8000™ Transfection Reagent (Beyotime, C0533) according to the manufacturer's instructions. For each well of a six-well plate, 2.5 μg plasmid DNA was mixed with 4 μL Lipo8000™ reagent and incubated for 15 min before addition to the cells. To generate stable cell lines, transfected cells were subjected to selection with either G418 (400 μg/mL; Sigma-Aldrich, A1720) or puromycin (1 μg/mL; Sigma-Aldrich, P4512) at 48 h after transfection. G418-resistant cells were selected for 1–2 weeks and subsequently maintained in medium containing 200 μg/mL G418. Puromycin-resistant cells were selected until all untransfected control cells were eliminated and subsequently maintained in medium containing 1 μg/mL puromycin. Antibiotic concentrations were determined by preliminary kill-curve assays.

2.3 SCAP constructs, mutagenesis and knockdown

Human SCAP cDNA was cloned into a Flag-tagged expression vector. The SCAP K210R mutant was generated by site-directed mutagenesis using the following primers: K210R-F, 5′-TGCAGACTTCAGCCACACTCAGAGACTTGTTATT-3′; and K210R-R, 5′-CAGGAACACCAAATAACAAGTCTCTGAGTGTGGC-3′. Synonymous nucleotide substitutions were introduced into the shRNA-targeted region to generate shRNA-resistant SCAP constructs without altering the encoded amino acid sequence. SCAP was depleted using a pLKO.1-based shRNA targeting human SCAP (5′-GCTCTGGTGTTCTTGGACAAA-3′). SCAP-depleted MDA-MB-231 cells were reconstituted with Flag-tagged shRNA-resistant SCAP WT or K210R, hereafter referred to as Flag-rSCAP WT and Flag-rSCAP K210R, respectively. SCAP knockdown and reconstitution were confirmed by immunoblotting, where Flag-SCAP denotes overexpression without endogenous SCAP depletion (Figs. 1c, 1e, 1f, 2b and 2c) and Flag-rSCAP denotes reconstitution after SCAP depletion (Figs. 2a, 2d, 2e and 3).

2.4 Sodium lactate treatment

For dose-response analysis, MDA-MB-231 cells were treated with sodium lactate at concentrations of 0, 5, 10, or 20 mmol/L for 24 h. Unless otherwise indicated, subsequent experiments were performed in the presence or absence of 20 mmol/L sodium lactate for 24 h. The working concentration was selected based on the tested dose range and previous studies employing high-millimolar sodium lactate

Uncorrected

concentrations to investigate lysine lactylation and related cellular responses (Zhang et al., 2019; Zong et al., 2024; Shao et al., 2025; Chen et al., 2024a). The 20 mmol/L condition represents a high-lactate experimental exposure rather than an exact reproduction of extracellular lactate concentrations in TNBC tumors. As the effects of lactate supplementation may be influenced by extracellular physicochemical conditions (Colegio et al., 2014), matched pH, sodium-ion, and osmolality controls were not included in the present experiments. Therefore, potential contributions from these factors could not be excluded.

2.5 Immunoprecipitation and immunoblotting

Cells were washed three times with ice-cold phosphate-buffered saline (PBS) and lysed for 30 min at 4 ℃ in lysis buffer containing 25 mmol/L Tris-HCl (pH 7.4), 150 mmol/L NaCl, 1% NP-40, 5 mmol/L EDTA, 10% glycerol, 50 mmol/L NaF, 1 mmol/L sodium orthovanadate (Na_3VO_4), and an EDTA-free protease inhibitor cocktail. Lysates were clarified by centrifugation at 15,000 × g for 20 min at 4 ℃, and protein concentrations were determined using a bicinchoninic acid (BCA) Protein Assay Kit (Pierce). Approximately 10% of each supernatant was retained as whole-cell lysate input. For endogenous SCAP immunoprecipitation, approximately 1.5 mg of total protein was incubated with an anti-SCAP antibody overnight, followed by incubation with agarose beads for 2 h. For Flag-SCAP immunoprecipitation, cell lysates were incubated with anti-Flag M2 agarose beads. The beads were washed five times with lysis buffer before elution. Immunoprecipitated proteins and input lysates were separated by sodium dodecyl sulfate–polyacrylamide gel electrophoresis (SDS-PAGE) and transferred to membranes. These were blocked with 3% bovine serum albumin (BSA) and incubated with the indicated primary antibodies followed by HRP-conjugated secondary antibodies. Immunoreactive signals were detected by chemiluminescence assay. SCAP lactylation was assessed by the immunoprecipitation of endogenous SCAP or Flag-SCAP followed by immunoblotting with a pan-Kla antibody. For the co-immunoprecipitation assays, INSIG1 recovered with Flag-rSCAP was examined by immunoblotting to compare the relative association of INSIG1 with SCAP under the indicated experimental conditions. Cell-based immunoprecipitation and immunoblot experiments were performed in three independent biological experiments; the discovery LC-MS/MS sample and pooled xenograft samples are described separately below.

2.6 Immunofluorescence microscopy and image analysis

Cells were fixed with 4% paraformaldehyde, permeabilized with 0.1% Triton X-100 for 5 min, and blocked with 3% bovine serum albumin for 1 h. Cells were incubated with an anti-SREBP1 antibody overnight at 4 ℃, followed by a fluorescent dye-conjugated secondary antibody and Hoechst 33342 staining. Images were acquired using a Leica TCS SP8 confocal microscope (Leica Microsystems, Germany) and analyzed with Fiji (ImageJ 1.53c). Nuclear SREBP1 fluorescence was quantified using Hoechst 33342-defined nuclear regions. For each condition in each independent experiment, 10 cells sampled from 3–4 microscopic fields were analyzed. Cell measurements were averaged within each experiment, and these experiment-level means were used for statistical analysis (n = 3 independent biological experiments).

2.7 Identification of SCAP K210 lactylation by LC-MS/MS

MDA-MB-231 cells expressing empty vector or Flag-SCAP were treated with or without 20 mmol/L sodium lactate for 24 h. Flag-SCAP was immunoprecipitated using anti-Flag beads, separated by SDS-PAGE, and visualized by Coomassie Brilliant Blue staining. The band at approximately 150 kDa was excised and subjected to in-gel digestion and LC-MS/MS by a commercial service provider. Peptides were separated on an EASY-nLC 1200 system using 0.1% formic acid in water as mobile phase A and 80% acetonitrile with 0.1% formic acid as mobile phase B at 400 nL/min. The gradient was 2–7% B from 0–1 min, 7–35% B from 1–36 min, 35–55% B from 36–45 min, 55–100% B from 45–52 min, and

Unedited

100% B from 52–60 min. Mass spectra were acquired on a Thermo Scientific Q Exactive HF-X in Top-20 data-dependent acquisition mode. Full MS scans covered m/z 350–1250 at a resolution of 60,000; the 20 most intense precursor ions were fragmented by higher-energy collisional dissociation (HCD) at normalized collision energy 27, with MS/MS acquired at a resolution of 15,000. Dynamic exclusion was 20 s. Spectra were searched using Proteome Discoverer 2.4 with Sequest HT (v1.17), Trypsin/P specificity, up to two missed cleavages, a precursor tolerance of 10 ppm, and fragment tolerance of 0.02 Da. The search result was based on one independently prepared biological sample (n = 1). The identified peptide TLQTSATLKDLLFGVPGK carried a +72.02113 Da modification assigned to peptide Lys9 (SCAP K210); the peptide-spectrum match had XCorr = 5.00, Percolator q-value = 0.0014, posterior error probability = 1.6×10^{-5}, and precursor mass error = −0.53 ppm. The annotated y9 and y10 ions support localization relative to the second lysine (SCAP K219), but the reported identification metrics are not site-localization probabilities.

2.8 Sequence alignment and SCAP topology annotation

SCAP amino acid sequences encompassing residues 203–217 from human, mouse, monkey, and pig were aligned using DNAMAN software to assess the conservation of the K210 residue. A schematic representation of SCAP membrane topology was generated to indicate the location of K210.

2.9 SRE luciferase reporter assay

MDA-MB-231 cells were seeded in 24-well plates and co-transfected with empty vector, Flag-SCAP WT, or Flag-SCAP K210R together with an SRE-driven luciferase reporter and a β-galactosidase control plasmid. After transfection, cells were treated with or without 20 mmol/L sodium lactate for 24 h. Luciferase and β-galactosidase activities were measured using the corresponding Promega assay systems. Luciferase activity was normalized to β-galactosidase activity and expressed as relative SRE luciferase activity. Three independent biological experiments were performed, each with four technical replicates per condition; technical replicates were averaged within each biological experiment before statistical analysis.

2.10 RNA extraction and reverse transcription quantitative PCR (RT-qPCR)

MDA-MB-231 cells expressing empty vector, Flag-SCAP WT, or Flag-SCAP K210R were treated with or without 20 mmol/L sodium lactate for 24 h. Total RNA was extracted using the TRIzol reagent (Invitrogen), and 1 μg of RNA was reverse-transcribed using TaqMan Reverse Transcription Reagents (Applied Biosystems). Quantitative PCR was performed using SYBR Premix Ex Taq (Takara) on a LightCycler 480 real-time PCR system. *FASN* and *SCD* transcript levels were normalized to α-tubulin and relative expression was calculated using the 2−ΔΔCt method, with the untreated empty-vector group as the calibrator. Four independent biological experiments were performed, each with technical triplicate measurements; technical replicates were averaged within each biological sample before analysis.

The primer sequences are listed below, where *SCD* encodes the SCD1 protein.

Table 1 Primer sequences used for reverse transcription quantitative PCR

Target	Forward primer (5′–3′)	Reverse primer (5′–3′)
FASN	CACAGGGACAACCTGGAGTT	ACTCCACAGGTGGGAACAAG
SCD	CGACGTGGCTTTTTCTTCTC	CCTTCTCTTTGACAGCTGGG
α-Tubulin	TATCGAGCGCCCAACCTACAC	CACCAGGTTGGTCTGGAATTCTGT

Unedited

2.11 BODIPY staining of neutral lipids

SCAP-depleted MDA-MB-231 cells reconstituted with Flag-rSCAP WT or Flag-rSCAP K210R were treated with or without 20 mmol/L sodium lactate for 24 h. Cellular neutral lipids were stained with BODIPY 493/503, and nuclei were counterstained with Hoechst 33342. Images were acquired under identical settings and analyzed using Fiji (ImageJ 1.53c). Lipid-droplet numbers were quantified from 10 cells sampled across 3–4 fields per condition in each of three independent biological experiments (n = 3); values were summarized at the experiment level before statistical analysis.

2.12 Xenograft model and DOX treatment

MDA-MB-231 cells depleted of SCAP and reconstituted with Flag-rSCAP WT or Flag-rSCAP K210R were used to establish subcutaneous xenografts in nude mice (1×10^6 cells per mouse). On Day 7 after inoculation, tumor volumes were measured before randomization. Within each genotype, mice were randomly assigned to vehicle or DOX groups while taking tumor size into account to balance pretreatment tumor volumes (six mice per group). Mice were numbered after allocation, then treatment was initiated. DOX was administered at 4 mg/kg by slow tail-vein injection on Days 7, 14 and 21 after inoculation. Tumor-volume measurements were performed by investigators blinded to vehicle-versus-DOX allocation. No exclusion criteria were prespecified, and no animals or measurements were excluded. Tumor dimensions were measured on Days 7, 10, 13, 16, 19, 22, and 25 after inoculation. Day 25 was the experimental endpoint; tumors were then excised, photographed and weighed. Day 0 refers to cell inoculation; measurements on Day 7 preceded the first DOX dose. For the tumor immunoprecipitation/immunoblot analysis, samples from the six mice in each group were combined into three non-overlapping pools, each containing samples from two different mice. Each pool was analyzed separately (n = 3 independent biological pools per group). All animal procedures were approved by the institutional animal care and use committee; identifying approval details are provided in the separate disclosure file for blinded review.

2.13 Statistical analysis

Statistical analyses were performed using GraphPad Prism 8.0.2 for cell-based and endpoint analyses; longitudinal repeated-measures analyses were implemented in Python using NumPy and SciPy. Data were presented as mean ± standard deviation (SD). Each independent cell experiment was the biological replicate for cell-based assays, and technical replicate measurements were averaged within each biological sample before analysis. For immunofluorescence and BODIPY assays, 10 cells sampled from 3–4 fields per condition were analyzed per independent experiment and summarized at the experiment level (n = 3). The luciferase assay comprised three independent biological experiments (n = 3), each with four technical replicates per condition; while RT-qPCR comprised four independent biological experiments (n = 4), each measured in technical triplicate. Cell-based immunoprecipitation/immunoblot experiments comprised three independent biological experiments. For Figure 3b, the experimental unit was an independent pool of samples from two mice (three pools per group). Each mouse was an independent experimental unit in the xenograft study (n = 6 per group); repeated measurements from a mouse were not treated as independent replicates. Cell-based experiments with genotype and sodium-lactate treatment as factors were analyzed by ordinary two-way ANOVA followed by Šídák-adjusted comparisons; the two conditions in Figure 1a were compared using a two-tailed paired t-test, paired by independent experiment. Longitudinal tumor volumes from Days 7–25 were analyzed by three-factor repeated-measures ANOVA, with genotype and DOX as between-mouse factors and measurement day as a categorical within-mouse factor matched by mouse identity. Natural-log-transformed volumes were used to assess relative growth profiles, with Greenhouse–Geisser corrections applied to time-containing effects; all 168 observations were included. Sensitivity analyses were performed by omitting Day 7 ($P = 0.0001225$) and by repeating the analysis on the raw-volume scale ($P = 0.09838$). Endpoint Day 25

Unedited

tumor volumes and tumor weights were each analyzed by two-way ANOVA with a genotype × DOX interaction term. All tests were two-sided, and $P < 0.05$ was considered statistically significant.

3 Results

3.1 Lactate-induced SCAP K210 Lactylation in TNBC cells

To determine whether lactate participates in regulating the SCAP–SREBP1 signaling axis, we first examined the subcellular distribution of SREBP1 following lactate treatment. Immunofluorescence showed that lactate treatment markedly enhanced the nuclear signal of SREBP1 in MDA-MB-231 cells (Fig. 1a), supporting a SREBP1-associated pathway response without directly measuring proteolytic processing or maturation.

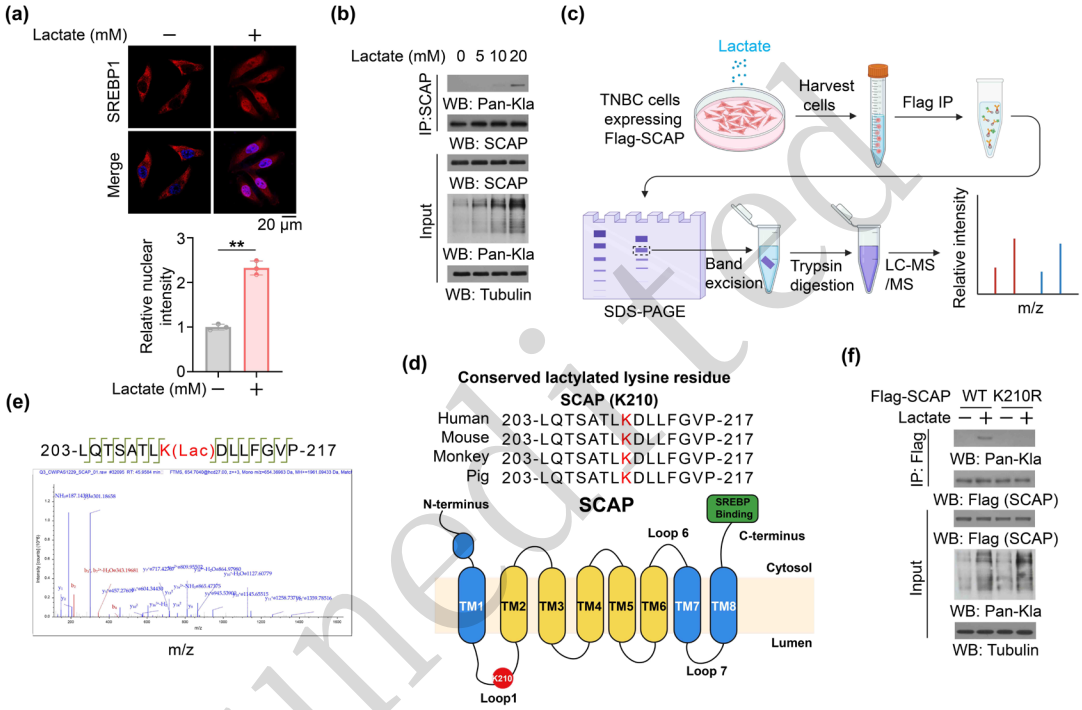


Fig. 1 Lactate Induces SCAP K210 Lactylation in TNBC cells

(a) MDA-MB-231 cells were treated with or without sodium lactate (20 mmol/L) for 24 h. Immunofluorescence staining was performed for SREBP1 (red), and nuclei were counterstained with Hoechst 33342 (blue). Representative images are shown. Scale bar, 20 μm. Nuclear SREBP1 signal was quantified from 10 cells sampled across 3–4 fields per condition in each of three independent biological experiments. Each plotted point represents one experiment-level mean (n = 3); data are expressed as mean ± SD and were analyzed using a two-tailed paired t-test, paired by experiment.

(b) MDA-MB-231 cells were treated with 0, 5, 10, or 20 mmol/L sodium lactate for 24 h. Endogenous SCAP was immunoprecipitated and analyzed by immunoblotting; whole-cell lysates served as input controls. Immunoprecipitation/immunoblot experiments were repeated independently three times (n = 3).

(c) Experimental workflow for Flag-SCAP immunoprecipitation, SDS-PAGE separation, Coomassie staining, excision of the SCAP-sized band, and LC-MS/MS analysis.

(d) Multiple-sequence alignment of SCAP amino acids 203–217 from human, mouse, monkey and pig, together with a schematic representation of SCAP topology, showing the conserved K210 residue.

(e) Annotated tandem mass spectrum for the peptide TLQTSATLK[+72.02113]DLLFGVPGK, corresponding to SCAP residues 202–219, with +72.02113 Da assigned to peptide Lys9 (SCAP K210). The annotated y9 and y10 ions support the K210 assignment relative to the C-terminal K219. The peptide-spectrum metrics were XCorr = 5.00, Percolator q = 0.0014, posterior error probability = 1.6×10^{-5}, and precursor mass error = −0.53 ppm. These metrics do not represent a site-localization probability.

Uncited

(f) MDA-MB-231 cells expressing Flag-SCAP WT or the K210R mutant were treated with or without sodium lactate (20 mmol/L) for 24 h. Flag-SCAP was immunoprecipitated, and immunoblotting was performed with the indicated antibodies. Whole-cell lysates were analyzed as input controls.
IP/WB experiments in B and F were independently repeated three times (n = 3); LC-MS/MS in E used one biological sample (n = 1). Kla, lysine lactylation; pan-Kla, pan-lysine lactylation; WT, wild type; IP, immunoprecipitation; WB, western blotting; LC-MS/MS, liquid chromatography–tandem mass spectrometry; SREBP1, sterol regulatory element-binding protein 1; SCAP, SREBP cleavage-activating protein; TNBC, triple-negative breast cancer; SD, standard deviation.

Given that SCAP is an essential upstream regulator of SREBP1 activation, we next examined whether SCAP undergoes lactate-responsive modification. Following the immunoprecipitation of SCAP, immunoblotting with a pan-lysine lactylation (pan-Kla) antibody revealed that SCAP-associated lactylation increased progressively with increasing lactate concentration, whereas total SCAP abundance remained unchanged (Fig. 1b). These findings indicate that lactate promotes SCAP-associated lysine lactylation. To identify lactylation sites on SCAP, we performed an LC-MS/MS analysis of Flag-SCAP immunoprecipitates (Fig. 1c). Mass spectrometric analysis identified lysine 210 (K210) as a lactylated residue on SCAP (Fig. 1d, e). Notably, K210 is highly conserved across species. The overexpression of the SCAP K210R mutant markedly reduced lactate-induced SCAP lactylation (Fig. 1f), supporting K210 as a lactate-responsive modification site.

3.2 Role of SCAP K210 in Lactate-Induced SREBP1 Signaling and Lipid Accumulation

To determine the functional significance of SCAP K210 lactylation, we depleted endogenous SCAP using short hairpin RNA (shRNA), reconstituted the cells with Flag-tagged shRNA-resistant SCAP (rSCAP), either wild-type (WT) or K210R, and compared their responses to lactate treatment. Lactate treatment markedly increased the nuclear accumulation of SREBP1 in WT cells, whereas this increase was substantially reduced in K210R-reconstituted cells (Fig. 2a). In separate overexpression experiments without endogenous SCAP depletion, lactate enhanced sterol regulatory element (SRE)-dependent reporter activity in Flag-SCAP WT-expressing cells, while the K210R mutation markedly impaired this transcriptional response (Fig. 2b). These results indicate that the identity of the residue at SCAP position 210 influences lactate-induced SREBP1-associated transcriptional responses. We next examined the downstream lipogenic program controlled by SREBP1. Lactate treatment increased the expression of the canonical SREBP1 target transcripts *FASN* and *SCD* (encoding SCD1) in Flag-SCAP WT-expressing cells, whereas Flag-SCAP K210R overexpression significantly attenuated their induction (Fig. 2c). In SCAP-depleted cells reconstituted with Flag-rSCAP, BODIPY staining further revealed increased neutral lipid accumulation and lipid droplet abundance following lactate treatment in WT cells, whereas these effects were markedly reduced in K210R-reconstituted cells (Fig. 2d).

Unedited

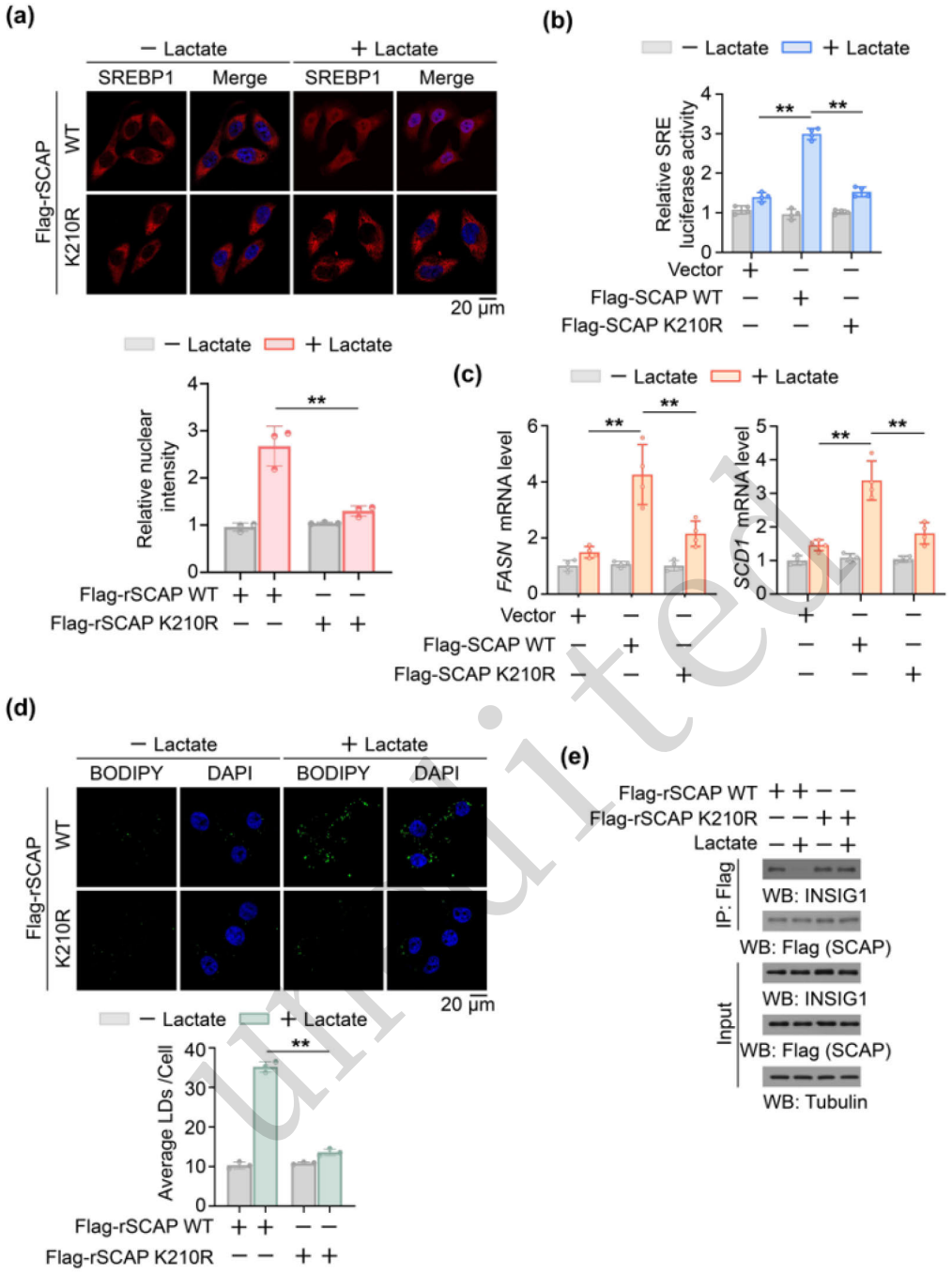


Fig. 2 Role of SCAP K210 in lactate-induced SREBP1 signaling and lipid accumulation

(a) SCAP-depleted MDA-MB-231 cells reconstituted with Flag-rSCAP WT or Flag-rSCAP K210R were treated with or without sodium lactate (20 mmol/L) for 24 h. Immunofluorescence staining was performed for SREBP1 (red), and nuclei were counterstained with Hoechst 33342 (blue). Representative images are shown. Scale bar, 20 μm. The nuclear SREBP1 signal was quantified from 10 cells across 3–4 fields per condition per independent experiment. Each point corresponds to one experiment-level mean (n = 3). Data are mean ± SD; ordinary two-way ANOVA with Šídák-adjusted comparisons was used.

(b) MDA-MB-231 cells expressing empty vector, Flag-SCAP WT, or Flag-SCAP K210R were transfected with an SRE-driven luciferase reporter and treated with or without sodium lactate (20 mmol/L) for 24 h. Each plotted point represents one independent biological experiment (n = 3); four technical replicates per condition were averaged within each

Unedited

experiment. Data are expressed as mean ± SD and were analyzed by ordinary two-way ANOVA with Šídák-adjusted comparisons.
(c) MDA-MB-231 cells expressing empty vector, Flag-SCAP WT, or Flag-SCAP K210R were treated with or without sodium lactate (20 mmol/L) for 24 h. *FASN* and *SCD* mRNA levels were normalized to α-tubulin and calculated by the $2^{-\Delta\Delta Ct}$ method, with the untreated empty-vector group as the calibrator. Each plotted point represents one independent biological experiment (n = 4); each sample was measured in technical triplicate, averaged before analysis. Data are expressed mean ± SD and were analyzed by ordinary two-way ANOVA with Šídák-adjusted comparisons.
(d) SCAP-depleted MDA-MB-231 cells reconstituted with Flag-rSCAP WT or Flag-rSCAP K210R were treated with or without sodium lactate (20 mmol/L) for 24 h. Neutral lipids were stained with BODIPY (green), and nuclei were counterstained with Hoechst 33342 (blue). Representative images are shown. Scale bar, 20 μm. Lipid droplet (LD) numbers were quantified from 10 cells across 3–4 fields per condition per independent experiment; each point represents an experiment-level mean (n = 3). Data are expressed mean ± SD; ordinary two-way ANOVA with Šídák-adjusted comparisons was used. LD counts indicate neutral-lipid accumulation and do not directly measure de novo lipid synthesis.
(e) SCAP-depleted MDA-MB-231 cells reconstituted with Flag-rSCAP WT or Flag-rSCAP K210R were treated with or without sodium lactate (20 mmol/L) for 24 h. Flag-rSCAP was immunoprecipitated and its association with INSIG1 was examined by immunoblotting. Whole-cell lysates were analyzed as input controls. The co-immunoprecipitation experiment was independently repeated three times (n = 3).
WT, wild type; rSCAP, shRNA-resistant SCAP; shRNA, short hairpin RNA; SRE, sterol regulatory element; SREBP1, sterol regulatory element-binding protein 1; SCAP, SREBP cleavage-activating protein; INSIG1, insulin-induced gene 1; FASN, fatty acid synthase; *SCD*, stearoyl-CoA desaturase gene (encoding SCD1); IP, immunoprecipitation; WB, western blotting; SD, standard deviation.

Given that SCAP activation is regulated by its interaction with INSIG1, we next examined whether K210 influences the interaction between SCAP and INSIG1. Co-immunoprecipitation analysis revealed that lactate reduced SCAP association with INSIG1 in WT cells, whereas this effect was diminished by the K210R mutation (Fig. 2e). Collectively, these findings suggest that SCAP K210 is involved in regulating lactate-induced SREBP1 signaling and neutral lipid accumulation.

3.3 SCAP K210 Regulates TNBC Xenograft Growth and Doxorubicin-Associated Responses In Vivo

To investigate the role of SCAP K210 in tumor growth and doxorubicin-associated responses in vivo, we established TNBC xenografts using SCAP-depleted MDA-MB-231 cells reconstituted with Flag-rSCAP WT or K210R. Subsequently, mice were assigned to vehicle or doxorubicin (DOX) treatment (Fig. 3a). The immunoprecipitation of SCAP followed by immunoblotting with a pan-Kla antibody revealed increased SCAP lactylation in DOX-treated WT tumors, whereas this increase was attenuated in K210R tumors(Fig. 3b). These results indicate that the K210R mutation attenuates the DOX-associated increase in SCAP lactylation signals in xenograft tumors.

Unedited

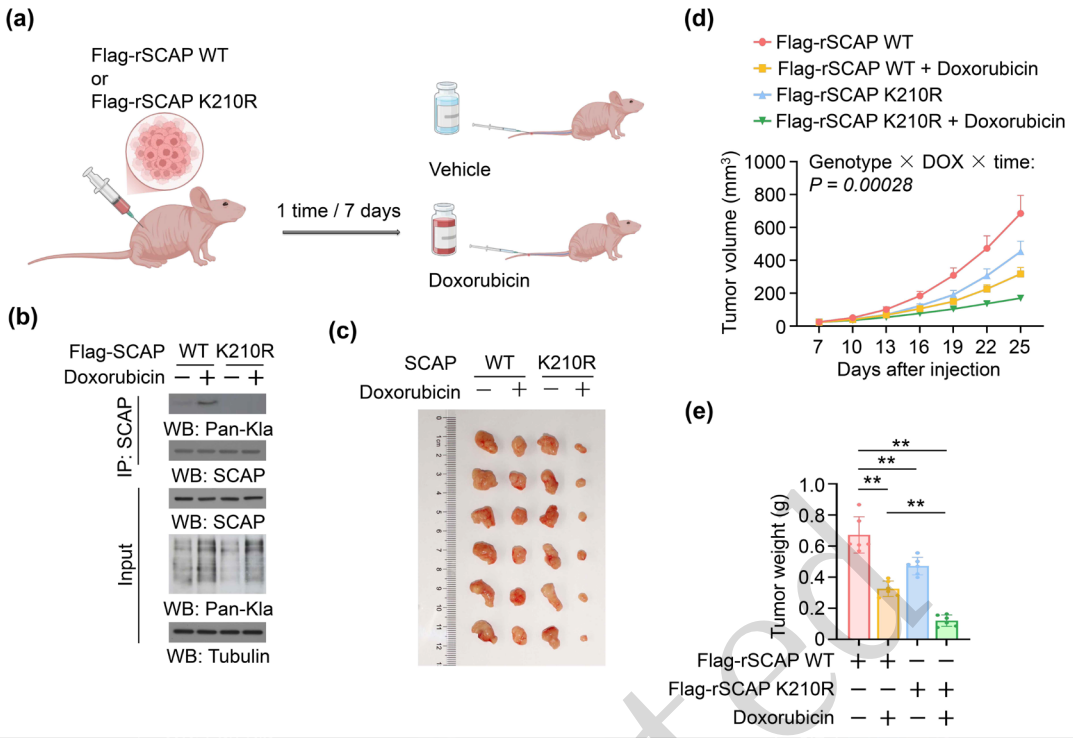


Fig. 3 SCAP K210 Regulates TNBC Xenograft Growth and Doxorubicin-Associated Responses In Vivo

(a) Schematic of the xenograft experimental design. SCAP-depleted MDA-MB-231 cells reconstituted with shRNA-resistant Flag-rSCAP WT or K210R were subcutaneously injected into mice (1×10^6 cells/mouse) on Day 0. On Day 7, mice were randomized within each genotype to vehicle or doxorubicin (DOX) treatment, taking baseline tumor volumes into account (n = 6 mice per group). DOX (4 mg/kg) was administered by slow tail-vein injection on Days 7, 14 and 21 after inoculation. Tumor volumes were measured by investigators blinded to treatment allocation.

(b) SCAP-associated lactylation in xenograft tumors. Tumor lysates were subjected to immunoprecipitation with an anti-SCAP antibody, followed by immunoblotting with anti-pan-Kla and anti-SCAP antibodies. Input lysates were analyzed as controls. For each group, tumor samples from six mice were combined into three non-overlapping biological pools (two mice per pool), each subjected to a separate IP/WB analysis (n = 3 independent pools per group).

(c) Representative images of excised xenograft tumors collected on Day 25.

(d) Tumor growth curves showing tumor volumes measured on Days 7, 10, 13, 16, 19, 22, and 25 after inoculation (n = 6 mice per group). Longitudinal tumor-volume data were analyzed by three-way repeated-measures ANOVA on natural log-transformed values, with SCAP genotype and DOX treatment as between-subject factors and time as the within-subject factor. Each mouse was treated as the repeated-measures unit, and Greenhouse–Geisser correction was applied (genotype × DOX × time interaction: $F(2.9287, 58.5735) = 7.5055$, $P = 0.0002758$). Curves show untransformed tumor volumes as mean ± SD.

(e) Tumor weights measured on Day 25 (n = 6 mice per group). Each point represents one mouse. Data were analyzed by ordinary two-way ANOVA (genotype × DOX interaction: $F(1, 20) = 0.0059$, $P = 0.9395$), followed by Šídák's multiple-comparisons test for the indicated pairwise comparisons. Data are presented as mean ± SD. *P < 0.05, **P < 0.01, ***P < 0.001, ****P < 0.0001; ns, not significant.

The xenograft study comprised a single cohort of 24 mice (n = 6 per group), and no animals were excluded from the analysis. SCAP, SREBP cleavage-activating protein; rSCAP, shRNA-resistant SCAP; shRNA, short hairpin RNA; WT, wild type; DOX, doxorubicin; pan-Kla, pan-lysine lactylation; IP, immunoprecipitation; WB, western blotting; SD, standard deviation; ANOVA, analysis of variance.

Under vehicle-treated conditions, K210R xenografts exhibited lower tumor volumes than WT xenografts (Fig. 3c–d). An analysis of longitudinal tumor-volume data using three-way repeated-measures ANOVA on natural log-transformed values revealed a significant genotype × DOX × time interaction, indicating differences in tumor-growth trajectories across the four experimental groups (Fig. 3d). Although K210R xenografts showed lower tumor volumes than WT xenografts under DOX

Uncorrected Proof

treatment, the genotype × DOX interaction in endpoint tumor volumes on Day 25 did not reach statistical significance. Similarly, endpoint tumor weights showed no significant genotype × DOX interaction ($F(1, 20) = 0.0059$, $P = 0.9395$; Fig. 3e). Collectively, these findings indicate that the SCAP K210 status is associated with xenograft growth and treatment-related growth profiles, while they do not establish a genotype-specific effect on DOX sensitivity.

3.4 Proposed Model linking SCAP K210 Lactylation to SREBP1-associated Signaling

In summary, our findings suggest a potential link between lactate-associated SCAP K210 lactylation, SREBP1-related lipid metabolic signaling, and tumor growth in TNBC. Sodium lactate exposure increased SCAP-associated lactylation signals, whereas the K210R mutation attenuated lactate-associated increases in the nuclear SREBP1 signal, SRE-dependent transcriptional activity, *FASN* and *SCD1* expression, and neutral-lipid accumulation. In xenograft models, the SCAP K210 status was associated with differences in basal tumor growth and longitudinal growth profiles under doxorubicin treatment. Based on these observations, we propose that SCAP K210 lactylation may modulate SCAP–INSIG1 association, potentially influencing ER-to-Golgi trafficking of the SCAP–SREBP complex and subsequent SREBP1 processing. These proposed intermediate steps were not directly examined in the present study. Although the longitudinal tumor-volume analysis revealed a significant genotype × DOX × time interaction, the endpoint analyses did not establish a genotype-specific effect on doxorubicin sensitivity. Together, these findings support a working model in which SCAP K210 lactylation is associated with SREBP1-related metabolic responses and tumor phenotypes (Fig. 4).

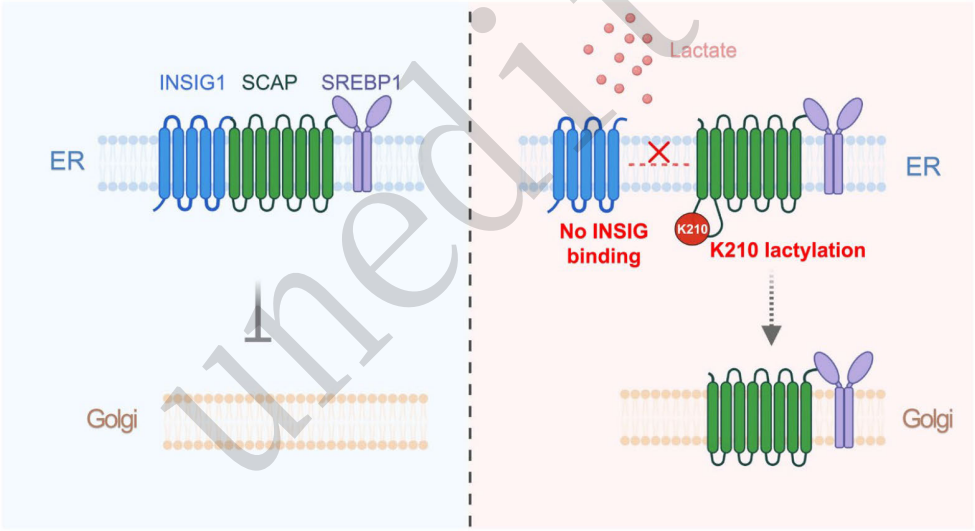


Fig. 4 Proposed Model linking SCAP K210 Lactylation to SREBP1-associated Signaling.Lactate-induced SCAP K210 lactylation is associated with reduced SCAP–INSIG1 association, increased SREBP1-related transcriptional activity, and neutral-lipid accumulation. The dashed arrows indicate proposed ER-to-Golgi trafficking and SREBP1 processing steps that were not directly assessed.

4 Discussion

The present study provides evidence that SCAP is a lactate-responsive non-histone lactylated protein and identifies K210 as a modified site in MDA-MB-231 cells. The attenuation of lactate-associated SRE reporter activity and *FASN* and *SCD1* expression by the K210R mutation connects this site to SREBP1-associated transcriptional responses. Quantified SREBP1 and BODIPY imaging, together with SCAP–

INSIG1 co-immunoprecipitation, further support a functional relationship between K210 and lipid-associated cellular phenotypes. In vivo, K210R reconstitution was associated with lower xenograft burden under both vehicle and doxorubicin treatment. While these findings support K210 lactylation as a regulatory component of the SCAP–INSIG1–SREBP1 axis, they leave the precise trafficking mechanism and its relationship with drug response unresolved.

SCAP classically regulates SREBP activation through its sterol-dependent association with INSIG1. Sterols promote SCAP–INSIG1 binding and ER retention, whereas the relief of this restraint permits SREBP processing (Yang et al., 2002). Glucose-dependent SCAP N-glycosylation and ammonia-induced SCAP–INSIG dissociation have shown that this checkpoint can also respond to non-sterol metabolic inputs (Cheng et al., 2015, 2022). The co-immunoprecipitation pattern in the present study is consistent with lactate-responsive K210 modification weakening SCAP retention by INSIG1. However, co-immunoprecipitation measures protein co-recovery rather than binding affinity or dissociation directly. Besides, SCAP localization, ER-to-Golgi transport, and proteolytic SREBP1 cleavage were not measured; therefore, altered trafficking remains a working model, and changes in SCAP conformation, stability, membrane organization, or interactions with additional partners may also be contributing factors. The SCAP/SREBP pathway has been recognized as an important regulator of lipid metabolic reprogramming in cancer. Cheng et al. (2018) highlighted the roles of SCAP/SREBP signaling in regulating lipid synthesis and uptake, supporting tumor growth, and providing potential targets for metabolic intervention. Within this framework, our findings suggest that SCAP K210 lactylation may represent an additional layer of metabolic regulation associated with SREBP1-related transcriptional responses. More recently, Zhu et al. (2025) linked SPRING lactylation to SCAP trafficking and SREBP regulation in AKT-hyperactivated intrahepatic cholangiocarcinoma. Therein, lactylation of a SCAP-associated regulatory protein was examined, while our investigation focuses on the K210 residue of SCAP itself in MDA-MB-231 cells, and the findings suggest potentially distinct mechanisms of lactylation-associated regulation within the SCAP/SREBP pathway. Nevertheless, the trafficking, SREBP processing and treatment-resistance mechanisms described in the SPRING model cannot be inferred from the present study without direct experimental validation.

Lysine lactylation was initially characterized on histones as a mechanism coupling glycolytic lactate production to transcription (Zhang et al., 2019), whereas subsequent studies have identified extensive non-histone lactylation and site-dependent regulation of protein activity (Yang et al., 2023). Alanyl-tRNA synthetases 1 and 2 (AARS1 and AARS2) can sense L-lactate and catalyze ATP-dependent lysine lactylation of intracellular substrates (Li et al., 2024). The present findings extend this regulatory framework to SCAP, though they do not identify the enzyme responsible for K210 lactylation. Whether AARS1, AARS2, or another lactyltransferase modifies SCAP remains unknown. In addition, K210R markedly attenuated rather than completely abolished the SCAP-associated Kla signal, indicating that other SCAP sites or background lactylated proteins may be involved. Although arginine preserves a basic side chain, K210R is not chemically equivalent to unmodified lysine and may influence local protein interactions independently of lactylation. Endogenous site editing and orthogonal site-specific quantification will therefore be required to strengthen a causal attribution. Genetic code expansion can introduce lactyllysine at defined protein sites in living cells (Shao et al., 2025). Such an approach would complement K210R substitution by more directly separating the effect of site-specific lactylation from that of amino acid replacement.

The effects of K210R on the SRE reporter and *FASN* and *SCD* transcripts are consistent with a SCAP lactylation role in lipid-metabolic regulation. SREBP-dependent lipid programs have previously been linked to breast cancer cell proliferation and cholesterol synthesis in TNBC models (Cai et al., 2019; Cheng et al., 2022). The present findings connect lactate availability with this lipid-regulatory pathway. Nevertheless, BODIPY staining measures the neutral-lipid pool and cannot determine whether the observed difference resulted from altered de novo synthesis, lipid uptake, oxidation, or storage.

Uncorrected

Although the imaging readouts were quantified, targeted lipidomics and isotope-tracing experiments will be necessary to establish the relevant metabolic fluxes.

Our xenograft findings suggest that the SCAP K210 status is associated with tumor burden in vivo. DOX treatment increased SCAP-associated pan-Kla signal in WT tumors, while the origin and mechanism of this change remain undetermined. K210R tumors had lower burden under vehicle conditions, and DOX reduced tumor burden in both genotypes; accordingly, the smaller K210R-plus-DOX tumors alone did not demonstrate enhanced drug sensitivity. Three-way repeated-measures ANOVA of log-transformed longitudinal tumor volumes revealed a significant genotype × DOX × time interaction, indicating differences in relative tumor-growth trajectories across the experimental groups. However, the genotype × DOX interaction did not reach statistical significance for endpoint tumor volumes, and likewise, endpoint tumor weights showed no significant interaction. These findings do not establish a genotype-specific effect on DOX sensitivity. Prior reports linking lipid metabolism to anthracycline response and lactylation of other proteins to DNA repair provide context but do not establish an equivalent mechanism for SCAP. SCAP K210 lactylation may contribute to doxorubicin resistance; however, this possibility remains hypothetical, as the current data do not establish a genotype-specific effect on doxorubicin sensitivity.

Several limitations define the scope of this study. First, the experiments were conducted primarily in a single TNBC cell line, and the in vivo analysis used subcutaneous xenografts in immunodeficient mice. The generality of the pathway across TNBC subtypes and its interaction with an intact immune microenvironment therefore remain unknown. Second, SREBP1 nuclear signal and BODIPY readouts were quantified from sampled cells and fields, whereas SCAP–INSIG1 co-immunoprecipitation provides a relative association readout rather than a direct measurement of binding affinity. Third, the LC-MS/MS discovery analysis used one independently prepared biological sample. Fourth, the K210R substitution may also affect protein properties or other modifications independently of lactylation. Fifth, matched pH, sodium-ion, and osmolality controls were not included for sodium lactate treatment; these contributions therefore cannot be excluded. Sodium lactate avoids the direct acid addition associated with lactic acid but does not itself establish specificity for lactate-dependent signaling. Validation in additional TNBC cell lines, endogenous K210-edited models, orthotopic or patient-derived tumors, and quantitatively resolved trafficking and lipid-flux assays will be required to establish the robustness and physiological relevance of this pathway.

From a translational perspective, the potential relevance of SCAP K210 lactylation should be considered within the evolving landscape of breast cancer biomarkers. Dai and Micsik (2026) reviewed emerging genomic, immune-related and circulating biomarkers that may contribute to molecular stratification and treatment decision-making in breast cancer. In contrast to these established and emerging biomarker categories, SCAP K210 lactylation may represent an exploratory metabolic marker reflecting lactate-associated alterations in SREBP-related signaling. However, the present study was limited to experimental models and did not evaluate SCAP K210 lactylation in clinical tumor specimens or establish associations with patient outcomes, thus its potential diagnostic, prognostic, or predictive value remains unknown. Future studies should develop reliable methods for a site-specific quantification of SCAP K210 lactylation and assess its prevalence, biological variability and clinical associations in independent TNBC patient cohorts. Such investigations will be necessary before considering its potential utility in patient stratification or treatment-response assessment.

5 Conclusions

This study identified SCAP as a lactate-responsive protein associated with lysine lactylation and K210 as a candidate major modified site. K210R attenuated sodium-lactate-associated SREBP1 nuclear signal,

Unedited

SRE-dependent transcription, *FASN* and *SCD1* expression, and neutral-lipid accumulation. The K210-dependent change in SCAP–INSIG1 co-recovery was consistent with altered regulation at the ER-retention checkpoint, but did not demonstrate ER-to-Golgi transport or SREBP1 proteolytic processing. In xenografts, K210R was associated with lower tumor burden, while longitudinal relative growth profiles differed by genotype and DOX treatment on the log scale; endpoint tumor weights did not show a significant genotype × DOX interaction.

These findings prompt further investigation of the SCAP K210–SREBP1 axis as a potential metabolic regulator in TNBC, while they do not establish SCAP K210 lactylation as a validated therapeutic target or demonstrate a genotype-specific doxorubicin-resistance effect. The identification of the responsible lactyltransferase, direct measurement of SCAP trafficking and lipid flux, and formal testing in additional TNBC models will be needed to determine the mechanism and generalizability of these observations.

Data availability statement

The data that support the findings of this study are available from the corresponding author upon reasonable request.

Acknowledgments

This work was supported by grants from the National Natural Science Foundation of China (82402048, Z.H.); and the Zhejiang Natural Science Foundation Discovery Project (LMS25H160018, Z.H.).

Author contributions

Z.H. conceived and designed the study and wrote the manuscript. Z.H. supervised the study. Z.H. and G.J. designed most of the experiments, performed the majority of the experiments, including cell biology, biochemical assays and animal studies, analyzed most of the data and wrote the manuscript. T.W., Y.Z., X.J., S.R., Y.L., Y.D., and Z.W. provided assistance throughout the study. G.J. performed statistical analysis and interpretation of the data. D.X. reviewed and edited the manuscript.

Compliance with ethics guidelines

Guimei JI, Ting WEN, Yudi ZHANG, Xiaoqian JIA, Shuo RU, Yingying LI, Yuran DUAN, Zheng WANG, Daqian XU, and Zhiqiang HU declare that they have no conflicts of interest.

All animal experiments were approved by the Institutional Animal Care and Use Committee of the First Affiliated Hospital, Zhejiang University School of Medicine (Approval No. 2024-1729 and No. 2025-256). All institutional and national guidelines for the care and use of laboratory animals were followed.

Declaration on the use of generative AI tools

During the preparation of this work, the authors used ChatGPT (OpenAI) to improve language and readability. After using this tool, the authors reviewed and edited the content as needed and take full responsibility for the content of the publication.

unedited

References

Asleh, K., Riaz, N., Nielsen, T.O., 2022. Heterogeneity of triple negative breast cancer: Current advances in subtyping and treatment implications. *Journal of Experimental & Clinical Cancer Research*, 41: 265. https://doi.org/10.1186/s13046-022-02476-1

Brown, M.S., Radhakrishnan, A., Goldstein, J.L., 2018. Retrospective on cholesterol homeostasis: The central role of Scap. *Annual Review of Biochemistry*, 87(1): 783-807. https://doi.org/10.1146/annurev-biochem-062917-011852

Cai, D., Wang, J., Gao, B., et al., 2019. ROR γ is a targetable master regulator of cholesterol biosynthesis in a cancer subtype. *Nature Communications,* 10: 4621. https://doi.org/10.1038/s41467-019-12529-3

Cai, X., Zhang, Z., Yang, X., et al., 2025. Unveiling the impact of lipid metabolism on triple-negative breast cancer growth and treatment options. *Frontiers in Oncology*, 15: 1579423. https://doi.org/10.3389/fonc.2025.1579423

Cancer Genome Atlas Network, 2012. Comprehensive molecular portraits of human breast tumours. *Nature*, 490: 61-70. https://doi.org/10.1038/nature11412

Chen, Y., Wu, J., Zhai, L., et al., 2024a. Metabolic regulation of homologous recombination repair by MRE11 lactylation. *Cell*, 187(2): 294-311.e21. https://doi.org/10.1016/j.cell.2023.11.022

Chen, S., Xu, Y., Zhuo, W., et al., 2024b. The emerging role of lactate in tumor microenvironment and its clinical relevance. *Cancer Letters*, 590: 216837. https://doi.org/10.1016/j.canlet.2024.216837

Chen, J., Huang, Z., Chen, Y., et al., 2025. Lactate and lactylation in cancer. *Signal Transduction and Targeted Therapy*, 10: 38. https://doi.org/10.1038/s41392-024-02082-x

Cheng, C., Ru, P., Geng, F., et al., 2015. Glucose-mediated N-glycosylation of SCAP is essential for SREBP-1 activation and tumor growth. *Cancer Cell*, 28(5): 569-581. https://doi.org/10.1016/j.ccell.2015.09.021

Cheng, C., Guo, J.Y., Geng, F., et al., 2016. Analysis of SCAP N-glycosylation and trafficking in human cells. *Journal of Visualized Experiments*, 117: e54709. https://doi.org/10.3791/54709

Cheng, C., Geng, F., Li, Z., et al., 2022. Ammonia stimulates SCAP/Insig dissociation and SREBP-1 activation to promote lipogenesis and tumour growth. *Nature Metabolism*, 4(5): 575-588. https://doi.org/10.1038/s42255-022-00568-y

Cheng, X., Li, J., Guo, D., 2018. SCAP/SREBPs are central players in lipid metabolism and novel metabolic targets in cancer therapy. *Current Topics in Medicinal Chemistry*, 18(6): 484-493. https://doi.org/10.2174/1568026618666180523104541

Colegio, O.R., Chu, N.Q., Szabo, A.L., et al., 2014. Functional polarization of tumour-associated macrophages by tumour-derived lactic acid. *Nature*, 513(7519): 559-563. https://doi.org/10.1038/nature13490

Dai, D.F., Micsik, T., 2026. Novel biomarkers in breast cancer for precision therapy and adaptive treatment strategies. *Advances in Translational Research*, 1(2): 179-192. https://doi.org/10.1556/1661.2026.00016

Dong, X., Tang, S., Chen, J., 2012. Dual functions of Insig proteins in cholesterol homeostasis. *Lipids in Health and Disease*, 11: 173. https://doi.org/10.1186/1476-511x-11-173

Faubert, B., Li, K., Cai, L., et al., 2017. Lactate metabolism in human lung tumors. *Cell*, 171(2): 358-371.e9. https://doi.org/10.1016/j.cell.2017.09.019

Garrido-Castro, A.C., Lin, N.U., Polyak, K., 2019. Insights into molecular classifications of triple-negative breast cancer: Improving patient selection for treatment. *Cancer Discovery*, 9(2): 176-198. https://doi.org/10.1158/2159-8290.cd-18-1177

Gu, X., Yang, J., Lai, R., et al., 2025. Impact of lactate on immune cell function in the tumor microenvironment: Mechanisms and therapeutic perspectives. *Frontiers in Immunology*, 16: 1563303. https://doi.org/10.3389/fimmu.2025.1563303

Ippolito, L., Comito, G., Parri, M., et al., 2022. Lactate rewires lipid metabolism and sustains a metabolic–epigenetic axis in prostate cancer. *Cancer Research*, 82(7): 1267-1282. https://doi.org/10.1158/0008-5472.can-21-0914

Izzo, L.T., Wellen, K.E., 2019. Histone lactylation links metabolism and gene regulation. *Nature*, 574(7779): 492-493. https://doi.org/10.1038/d41586-019-03122-1

Jin, H., Wang, J., Wang, Z., et al., 2023. Lipid metabolic reprogramming in tumor microenvironment: From mechanisms to therapeutics. *Journal of Hematology & Oncology*, 16: 103. https://doi.org/10.1186/s13045-023-01498-2

Lehmann, B.D., Jovanović, B., Chen, X., et al., 2016. Refinement of triple-negative breast cancer molecular subtypes: Implications for neoadjuvant chemotherapy selection. *PLOS ONE*, 11(6): e0157368. https://doi.org/10.1371/journal.pone.0157368

Li, Y., Sun, F., Li, C., et al., 2023. RARRES2 regulates lipid metabolic reprogramming to mediate the development of brain metastasis in triple negative breast cancer. *Military Medical Research*, 10: 34. https://doi.org/10.1186/s40779-023-00470-y

Li, H., Liu, C., Li, R., et al., 2024. AARS1 and AARS2 sense l-lactate to regulate cGAS as global lysine lactyltransferases. *Nature*, 634(8036): 1229-1237. https://doi.org/10.1038/s41586-024-07992-y

Li, J., Shang, Y., Wu, H., et al., 2026. Lysine lactylation-mediated post-translational modification: Molecular mechanisms and therapeutic target exploration in tumour drug resistance. *Clinical and Translational Medicine*, 16(6): e70714. https://doi.org/10.1002/ctm2.70714

Liang, L., Zhao, L., Yu, B., et al., 2023. Caffeic acid phenethyl ester reverses doxorubicin resistance in breast cancer cells via lipid metabolism regulation at least partly by suppressing the Akt/mTOR/SREBP1 pathway. *The Kaohsiung Journal of Medical Sciences*, 39: 605-615. https://doi.org/10.1002/kjm2.12675

Luqmani, Y.A., 2026. Lactate, a spearhead of cancer aggressiveness: Metabolic reprogramming, immune suppression, and metastatic progression. Medical Principles and Practice. *Advance online publication*, 8 May 2026. https://doi.org/10.1159/000552146

Marra, A., Trapani, D., Viale, G., et al., 2020. Practical classification of triple-negative breast cancer: Intratumoral heterogeneity, mechanisms of drug resistance, and novel therapies. *npj Breast Cancer*, 6: 54. https://doi.org/10.1038/s41523-020-00197-2

Mehanna, J., Haddad, F.G., Eid, R., et al., 2019. Triple-negative breast cancer: Current perspective on the evolving therapeutic landscape. *International Journal of Women's Health*, 11: 431-437. https://doi.org/10.2147/ijwh.s178349

Uncorrected

Menendez, J.A., Lupu, R., 2017. Fatty acid synthase (FASN) as a therapeutic target in breast cancer. *Expert Opinion on Therapeutic Targets*, 21(11): 1001-1016. https://doi.org/10.1080/14728222.2017.1381087

Munkácsy, G., Santarpia, L., Győrffy, B., 2023. Therapeutic potential of tumor metabolic reprogramming in triple-negative breast cancer. *International Journal of Molecular Sciences*, 24(8): 6945. https://doi.org/10.3390/ijms24086945

Nedeljković, M., Damjanović, A., 2019. Mechanisms of chemotherapy resistance in triple-negative breast cancer—How we can rise to the challenge. *Cells*, 8(9): 957. https://doi.org/10.3390/cells8090957

Nuzzo, P.V., Rodrigues, S., Ribeiro, C.F., et al., 2025. Targeting cancer metabolism: Therapeutic potential of the fatty acid synthase (FASN) inhibitors. *Critical Reviews in Oncology/Hematology*, 214: 104910. https://doi.org/10.1016/j.critrevonc.2025.104910

Peng, X., Du, J., 2025. Histone and non-histone lactylation: Molecular mechanisms, biological functions, diseases, and therapeutic targets. *Molecular Biomedicine*, 6: 38. https://doi.org/10.1186/s43556-025-00275-6

Shao, C., Tang, S., Yu, S., et al., 2025. Genetic code expansion reveals site-specific lactylation in living cells reshapes protein functions. *Nature Communications*, 16(1): 227. https://doi.org/10.1038/s41467-024-55165-2

Singh, L., Nair, L., Kumar, D., et al., 2023. Hypoxia induced lactate acidosis modulates tumor microenvironment and lipid reprogramming to sustain the cancer cell survival. *Frontiers in Oncology*, 13: 1034205. https://doi.org/10.3389/fonc.2023.1034205

Sirois, I., Aguilar-Mahecha, A., Lafleur, J., et al., 2019. A unique morphological phenotype in chemoresistant triple-negative breast cancer reveals metabolic reprogramming and PLIN4 expression as a molecular vulnerability. *Molecular Cancer Research*, 17: 2492-2507. https://doi.org/10.1158/1541-7786.MCR-19-0264

Sun, L., Li, L., Goldstein, J.L., et al., 2005. Insig required for sterol-mediated inhibition of Scap/SREBP binding to COPII proteins in vitro. *Journal of Biological Chemistry*, 280(28): 26483-26490. https://doi.org/10.1074/jbc.m504041200

Sun, Y., Wang, H., Cui, Z., et al., 2025. Lactylation in cancer progression and drug resistance. *Drug Resistance Updates*, 81: 101248. https://doi.org/10.1016/j.drup.2025.101248

Taborda Ribas, H., Sogayar, M.C., Dolga, A.M., et al., 2024. Lipid profile in breast cancer: From signaling pathways to treatment strategies. *Biochimie*, 219: 118-129. https://doi.org/10.1016/j.biochi.2023.11.008

Tan, Z., Deme, P., Boyapati, K., et al., 2023. Key regulator PNPLA8 drives phospholipid reprogramming induced proliferation and migration in triple-negative breast cancer. *Breast Cancer Research*, 25: 148. https://doi.org/10.1186/s13058-023-01742-0

Tracz-Gaszewska, Z., Dobrzyn, P., 2019. Stearoyl-CoA desaturase 1 as a therapeutic target for the treatment of cancer. *Cancers*, 11(7): 948. https://doi.org/10.3390/cancers11070948

Wang, Z., Jiang, Q., Dong, C., 2020. Metabolic reprogramming in triple-negative breast cancer. *Cancer Biology and Medicine*, 17(1): 44-59. https://doi.org/10.20892/j.issn.2095-3941.2019.0210

Xu, D., Wang, Z., Xia, Y., et al., 2020. The gluconeogenic enzyme PCK1 phosphorylates INSIG1/2 for lipogenesis. *Nature*, 580(7804): 530-535. https://doi.org/10.1038/s41586-020-2183-2

Yamauchi, Y., Furukawa, K., Hamamura, K., et al., 2011. Positive feedback loop between PI3K-Akt-mTORC1 signaling and the lipogenic pathway boosts Akt signaling: Induction of the lipogenic pathway by a melanoma antigen. *Cancer Research*, 71(14): 4989-4997. https://doi.org/10.1158/0008-5472.can-10-4108

Yang, T., Espenshade, P., Wright, M., et al., 2002. Crucial step in cholesterol homeostasis: Sterols promote binding of SCAP to INSIG-1, a membrane protein that facilitates retention of SREBPs in ER. *Cell*, 110(4): 489-500. https://doi.org/10.1016/S0092-8674(02)00872-3

Yang, Z., Yan, C., Ma, J., et al., 2023. Lactylome analysis suggests lactylation-dependent mechanisms of metabolic adaptation in hepatocellular carcinoma. *Nature Metabolism*, 5(1): 61-79. https://doi.org/10.1038/s42255-022-00710-w

Yi, J., Zhu, J., Wu, J., et al., 2020. Oncogenic activation of PI3K-AKT-mTOR signaling suppresses ferroptosis via SREBP-mediated lipogenesis. *Proceedings of the National Academy of Sciences*, 117(49): 31189-31197. https://doi.org/10.1073/pnas.2017152117

Yu, L., Wei, W., Lv, J., et al., 2024. FABP4-mediated lipid metabolism promotes TNBC progression and breast cancer stem cell activity. *Cancer Letters*, 604: 217271. https://doi.org/10.1016/j.canlet.2024.217271

Zhang, D., Tang, Z., Huang, H., et al., 2019. Metabolic regulation of gene expression by histone lactylation. *Nature*, 574(7779): 575-580. https://doi.org/10.1038/s41586-019-1678-1

Zhang, K., Guo, L., Li, X., et al., 2025a. Cancer-associated fibroblasts promote doxorubicin resistance in triple-negative breast cancer through enhancing ZFP64 histone lactylation to regulate ferroptosis. *Journal of Translational Medicine*, 23: 247. https://doi.org/10.1186/s12967-025-06246-3

Zhang, D., Liang, C., Wu, C., et al., 2025b. Nonhistone lactylation: A hub for tumour metabolic reprogramming and epigenetic regulation. *Journal of Translational Medicine*, 23: 901. https://doi.org/10.1186/s12967-025-06813-8

Unedited

Zhao, Q., Lin, X., Wang, G., 2022. Targeting SREBP-1-mediated lipogenesis as potential strategies for cancer. *Frontiers in Oncology*, 12: 952371. https://doi.org/10.3389/fonc.2022.952371

Zhu, J., Xiong, Y., Zhang, Y., et al., 2025. Simvastatin overcomes the pPCK1-pLDHA-SPRINGlac axis-mediated ferroptosis and chemo-immunotherapy resistance in AKT-hyperactivated intrahepatic cholangiocarcinoma. *Cancer Communications*, 45(8): 1038-1071. https://doi.org/10.1002/cac2.70036

Zong, Z., Xie, F., Wang, S., et al., 2024. Alanyl-tRNA synthetase, AARS1, is a lactate sensor and lactyltransferase that lactylates p53 and contributes to tumorigenesis. *Cell*, 187(10): 2375-2392.e33. https://doi.org/10.1016/j.cell.2024.04.002

unedited